Flame speed enhancement of a nitrocellulose monopropellant using graphene microstructures

S. Jain, W. Park, Y. P. Chen, and L. Qiao

Citation: Journal of Applied Physics **120**, 174902 (2016); doi: 10.1063/1.4966933
View online: http://dx.doi.org/10.1063/1.4966933
View Table of Contents: http://scitation.aip.org/content/aip/journal/jap/120/17?ver=pdfcov
Published by the AIP Publishing

Flame speed enhancement of a nitrocellulose monopropellant using graphene microstructures

S. Jain,[1] W. Park,[2] Y. P. Chen,[3] and L. Qiao[1,a)]
[1]*School of Aeronautics and Astronautics Engineering, Purdue University, West Lafayette, Indiana 47907, USA*
[2]*School of Electrical and Computer Engineering, Purdue University, West Lafayette, Indiana 47907, USA*
[3]*Department of Physics and Astronomy, Purdue University, West Lafayette, Indiana 47907, USA*

(Received 28 July 2016; accepted 20 October 2016; published online 3 November 2016)

The control and enhancement of the combustion wave propagation velocities of solid monopropellants are very important for the development of low cost and efficient micro power systems such as microthrusters and thermal-to-electrical energy conversion devices. In this work, the flame speed enhancement of a nitrocellulose (NC) solid monopropellant using highly conductive graphene structures was demonstrated. Two different graphene structures, namely, graphene foam (GF) and graphene nano-pellets (GNPs), were studied. For the GNP-doped NC films, fuel layers $500 \pm 30\,\mu$m thick were deposited and the doping concentrations were varied from 1% to 5% by mass. For the GF, the fuel loading ratio (%) and the foam density were varied to study their effect on the flame speed propagation behavior. Self-propagating combustion waves were observed, with average flame speed enhancements up to 8 times the bulk value. The flame speed enhancement, for both the GNPs and the GF, showed a parabolic trend as a function of their concentrations, and an optimum value for each case was determined. However, the flame speed enhancement, as a function of the GF density (for a fixed fuel loading ratio), showed a monotonic decreasing trend. Moreover, the reusability of the GF structures was also tested by re-depositing them with fuel after combustion. Similar flame speed enhancement was obtained using the fresh and the re-used GF structures. *Published by AIP Publishing.* [http://dx.doi.org/10.1063/1.4966933]

I. INTRODUCTION

A number of studies have been performed to augment the burning rate of solid propellants by either adding metal/metal oxide additives or varying the fuel/oxidizer particle size. Beckstead *et al.*[1] modeled the burning rate of 87.4% ammonium perchlorate (AP)/HTPB system at 68 atm and found the burning rate to increase from 0.7 cm/s to 5 cm/s as the AP particle size was decreased from 1000 μm to 10 μm. Shalom *et al.*[2] showed that the burning rate of the composite propellant (Al/AP/HTPB) system containing 18% Al is enhanced by 84% at pressures of around 10 MPa when 9% of the coarse aluminum powder was replaced by the nano-aluminum powder. Burning rate modifiers, mostly in the form of catalyst, could also be added to the composite propellant systems to assist in the decomposition of either the binder or the oxidizer. Since the added catalysts did not decompose or ignite, they reduced the net ISP (specific impulse) of the system.[3–13] These catalysts were introduced in either liquid or solid form and were usually oxides of the transition metals such as Ag, Cu, Fe, Cd, Mg, Zn, and Li (TMO).[14] Nevertheless, the addition of metals in the propellant mixture has several disadvantages: (1) the propellant mixture is more sensitive to accidental initiation due to impact, friction, spark, flame, or heat;[14] (2) the condensed solid metal particles in the exhaust being detrimental to the hardware because of their abrasive action; and (3) the toxic exhausts from the combustion of metals. These disadvantages could be either avoided or at minimum reduced by using the graphene structures. Since the graphene structures usually do not participate in the combustion process, no solid particles or toxic gases are produced.[15]

Carbon-based materials, such as carbon nanotubes (CNTs),[16] graphene nano-pellets (GNPs),[17] and graphene foams (GFs),[18] because of their high thermal (1600–4600 W/mK)[19–24] and electrical conductivity,[18,25,26] mechanical strength, optical properties, and large surface-to-volume ratio, have been used as nano-fillers to enhance the thermal conductivity of various composites,[18,27–43] as thermal interface materials[44–47] and as heat exchangers in nano-electronic devices.[48,49] They also have applications in polymer fabrication, biomedicine, organic synthesis, catalysis, and sensors.[50–57] Yu *et al.*[30] showed that the thermal conductivity of pure epoxy could be increased by 3000% by using GNPs at 25% volumetric loading. They also conducted experiments with single-walled carbon-nanotubes (SWCNTs) but found the amount of enhancement to be half of that of the GNPs. Goyal[28] also showed that the thermal conductivity of pure epoxy could be increased by 500% using hybrid graphene-metal particles at 5% volumetric loading. Similar enhancements were also reported by Shahil,[32] where they found the thermal conductivity of epoxy to be increased by 2300% by using mixed monolayer and multilayer graphene at 10% volumetric loading. Several studies have also been performed to test the effect of the GF on the thermal conductivity of the composites. Zhao *et al.*[38] showed that the thermal conductivity of the PDMS (polydimethylsiloxane) polymer could be increased 3-fold by using GF. Liu *et al.*[36] and Chen

a)Author to whom correspondence should be addressed. Electronic mail: lqiao@purdue.edu. Tel.: (765)494-2040.

et al.[18] showed that the thermal diffusivity of pure epoxy could be increased 10 and 46 times using GF at 5% and 9% by weight, respectively.

However, there exists contradiction in the literature on the effects that the CNT addition has on the thermal conductivity of the composites. Huang *et al.*[29] conducted experiments with vertically aligned CNTs and found the thermal conductivity of polymer/CNT complex to be increased by 280% at 0.3% weight fraction. However, Bonnet *et al.*[58] found only a slight increase in the thermal conductivity, around 55%, using CNTs at 7% by volume. An opposite trend was observed by Moisala *et al.*,[59] where the thermal conductivity of the epoxy/CNT composites decreased with the addition of SWCNTs. A major limitation of using the carbon-nanotubes is the thermal contact resistance at their interface with both the medium and adjacent nanostructures.[60–65] The thermal boundary resistance (TBR) for CNTs has been reported to be between 0.07 and 0.8 cm^2/kW.[60,66–68] A TBR value of 0.04 cm^2/kW was reported by Zhang *et al.*[35] for the GF. The thermal contact resistance is greatly reduced in the GF because of its three-dimensional network of covalently bonded two-dimensional graphene structures.[41] The high thermal resistance in the CNTs could be attributed either to the high Kapitza resistance[61] due to the mismatch between the phonon density of states (DOS) between the 1-D CNTs and the 3-D bulk material or to the lack of thermal percolation in CNT composites.[62] Park *et al.*[47] reported a TBR value of 0.043 cm^2/kW for the FLG (few layer graphene), whereas Raza *et al.*[69] and Shen *et al.*[70] reported TBR values of around 0.1 cm^2/kW and 0.3 cm^2/kW for the GNPs, respectively. Thus, the thermal contact resistance of the GNPs could be expected to lie somewhere between that of the CNTs and the GF. A comprehensive study was performed by Ji *et al.*,[34] in which the thermal conductivity enhancement of wax using GF, GNPs, and CNTs was compared. The thermal conductivity of the composite increased by 18 (1% vol.), 11 (4% vol.), and 6 (10% vol.) times using GF, GNPs, and CNTs, respectively.

In addition to enhancing the thermal conductivity, these carbon nanomaterials have also been shown to augment the burning rate of various solid monopropellants. Since the burning rate of solid monopropellants is controlled by heat transport (from burned to unburned material), it depends on the thermal conductivity of the propellants[71,72] and thus could be enhanced by coupling these solid propellants to highly conductive graphene structures. Most of the solid monopropellants have a thermal conductivity in the range of 0.1–1 W/mK,[73] which is much lower than that of the carbon-based materials (as high as a few thousand W/mK). Choi *et al.*[15] showed that the flame speed of a solid monopropellant TNA (trinitramine) could be enhanced by 10^4 times by coupling it to the MWCNTs (multi-wall carbon nanotubes) at nanoscale. Furthermore, in our previous work,[74] graphite sheets were used to enhance the burning rate of a solid monopropellant. Flame speed enhancements up to 4 times were obtained. Zhang *et al.*[75] also studied the effect of graphene oxides (GOs) on the burning rate of nitrocellulose (NC) and significant enhancements up to 7 times the bulk value were observed.

In this work, GF and GNPs were chosen to be the thermally conductive fillers to solid propellants because of their unique thermal properties as described above. Their ability to enhance the burning rates of solid propellants has not been explored previously. An experiment was developed to measure the flame speeds of a monopropellant nitrocellulose (NC) which was either doped with GNPs or filled in the GF matrix. For the GNPs, the amount of GNPs added to NC was varied, whereas for the GF, both the NC loading ratio (%) and the GF density were varied. An optimum loading ratio for both the GNPs and the GF was determined. The reusability of the GF structures was also tested, and similar flame speed enhancement was obtained using the fresh and the reused GF structures.

II. EXPERIMENTAL METHOD

A. Material selection

Nitrocellulose ($C_6H_8(NO_2)_2O_5$), with a nitration level of 10.9%–11.2%, was selected as the solid fuel because of its ease of combustion at atmospheric conditions and wide use as an energetic polymeric binder in the nitrocellulose-based propellants in solid rocket motors. In addition, the nitration level of the solid propellant is such that it exhibits deflagration and not detonation during combustion. The nitrocellulose solution (6% in ethanol/diethyl ether) was purchased from Sigma-Aldrich, which was then further diluted using acetone, giving the net NC solution to be 4% by weight.

GNPs (graphene nano-pellets) and GF were used as the conductive materials. The GNPs were less than 3 nm thick (3–8 graphene monolayers) with lateral dimensions ranging between 2 and 8 μm, whereas the GF was 3 mm thick and had an average porosity of 99.2%. The foam density was varied from 8 mg/cm^3 to 40 mg/cm^3 to study its effect on the average flame speed enhancements. For all the experiments conducted, the dimensions of the foam sheet and the GNP-doped fuel layer were kept constant to 2.5 cm × 0.6 cm. This was done to make sure that the length of the samples was much greater than the width so that the flame fronts obtained were nearly planar.

B. Sample preparation

For the GNPs-doped NC films, the GNPs (A-12-25 G, Graphene Laboratories) were added to the base NC solution at various concentrations ranging from 1% to 5% of the NC weight. An ultrasonic disruptor was used to disperse the GNPs evenly in the base NC solution and to minimize agglomeration. A series of four-second-long and four-second apart pulses were used for 8 min. The GNP/NC solution was then drop-casted onto a thermally insulating glass slide (2.5 cm long and 0.6 cm wide) and evaporated at ambient conditions leaving an adhesive coating of GNP-NC behind. For all the cases tested, the GNP-doped fuel layers had a thickness of 500 ± 30 μm as shown in Fig. 1(a).

The GF, following the method outlined by Chen *et al.*,[18] was grown on a Ni template (3 mm-thick open-cell foam with 75 pores per inch) by the chemical vapor deposition (CVD) method with flowing a gas mixture of CH_4 (20 sccm),

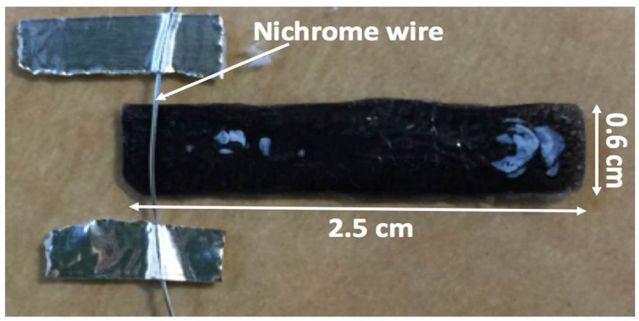

(a)

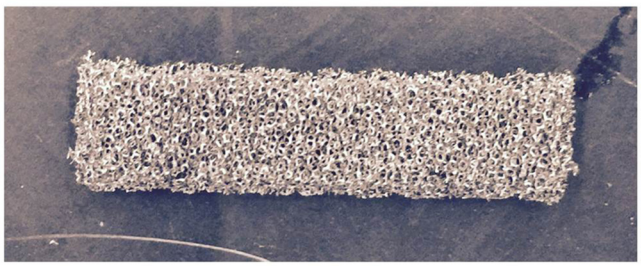

(b)

FIG. 1. (a) Experimental set-up of a typical sample (GNP-doped NC film, 5% by weight). (b) GF sheet before fuel addition.

H_2 (20 sccm), and Ar (210 sccm) at 1050 °C for 1–3 h. The exact growth time controlled the density of the GF. The uncertainty associated with the obtaining the GF density was $\pm 2\,mg/cm^3$. After the growth process, the GF/Ni surface was drop-casted with a polymethyl methacrylate (PMMA) solution to protect the structure from the vigorous etching process. The Ni template was then etched out by first using a $Fe(NO_3)_3$ solution (1 M) at 90 °C for 2 days and then using a HCl (1 M) solution at 90 °C for next 2 days. After the etching process, the samples were rinsed with deionized water and then hot acetone to completely dissolve the PMMA. The final GF sheet cut in the required dimension of 2.5 cm $\times$ 0.6 cm is shown in Fig. 1(b). The pure NC solution (4% by weight) was then drop-casted onto the foam sheet surface, at various amounts to get the desired fuel loading ratio %. After the GF surface was drop-casted with the pure NC solution, the GF/NC samples were left to dry in the ambient conditions for 24 h, which gave enough time for all the solvents (acetone) to completely evaporate. Moreover, special attention was paid to the fluctuations observed while measuring the sample weight (before ignition). If the fluctuations observed were significant, then the samples were left to dry for a longer time. The samples were considered dried only when there were no fluctuations in the weight measurement and a constant weight was achieved. Moreover, the thermogravimetric analysis (TGA) of GF before and after fuel addition was conducted, up to 100 °C at a rate of 10 °C/min, to make sure that there was no residual solvent (acetone) prior to combustion. The GF-NC sample was evaporated at the ambient conditions for 24 h before conducting the TGA analysis. Negligible loss (<1%) in the GF-NC sample mass was observed, thus confirming that there is no residual solvent after the evaporation process. The ignition of the samples was achieved by using a resistive heating nichrome wire, as shown in Fig. 1(a). A constant voltage was applied across the wire to ignite the fuel samples.

C. Flame speed determination

Figure 2 shows the snapshots of the reaction propagation wave at different times along the sample. The flame speed was determined by using the algorithm developed in our previous study,[74] in which the brightest peak of the luma profile was tracked. An infrared camera (FLIR-SC6100) was used to capture these luma profiles and the flame propagation. Based on the spatial and the temporal uncertainty of 2% and 6%, respectively, the net uncertainty in the determining the flame speeds came out to be less than 6.5%. No quantitative temperature measurements were done for the flame speed calculations, but only the intensities of the luma profiles were used. A K-type thermocouple, embedded in the fuel surface, was used to measure the peak surface temperature. An average peak temperature of 600 K was obtained with a standard deviation of ± 10 K.

III. RESULTS AND DISCUSSION

A. Microscopy investigation

Figure 3 shows the SEM (scanning electron microscopy) images of the pure and the GNPs-doped NC films. As can been seen from Fig. 3(a), the surface of the pure NC film was quite smooth and continuous, which was consistent with the adhesive nature of the NC coating. However, after adding the GNPs, the surface roughness increases and a highly porous network was obtained, as can be seen from Figs. 3(b) and 3(c). In addition, the amount of surface roughness was found to increase with the weight percent of the GNPs added. This was consistent with the work performed by Zhang *et al.*[75] in which a similar trend of increasing roughness with increasing graphene oxide (GO) weight concentration was observed.

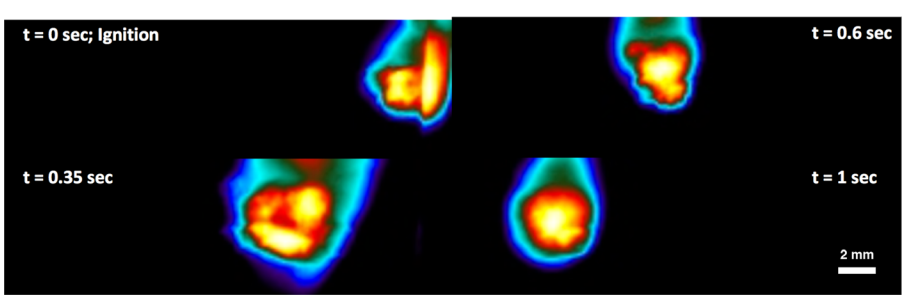

FIG. 2. Ignition and flame propagation along a typical sample. The case shown corresponds to 5% by weight 500 μm thick GNP-doped NC film.

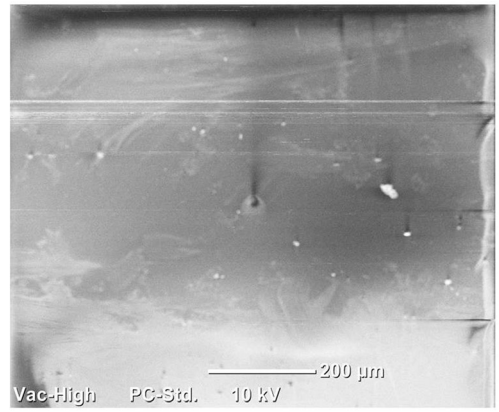

(a)

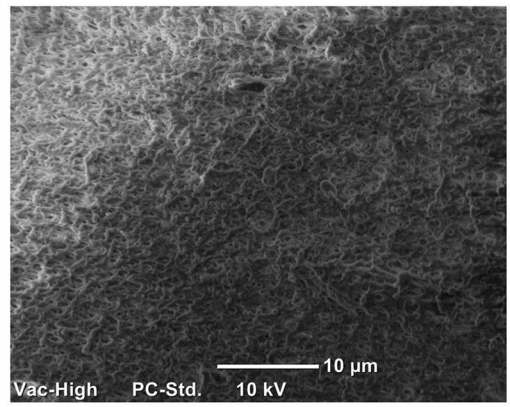

(b)

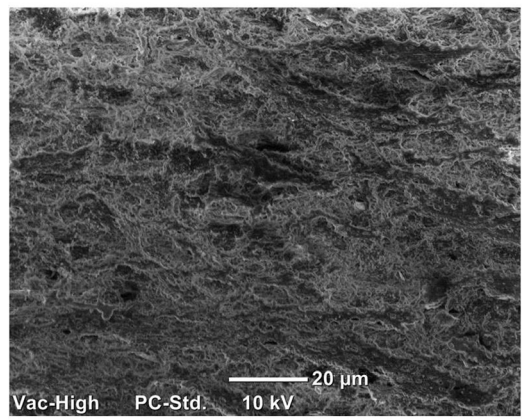

(c)

FIG. 3. SEM image of (a) pure NC film (b) 3% and (c) 5% GNPs-doped NC film.

Figure 4 shows the three dimensional, interconnected, highly porous graphene structure before the fuel deposition. The GF exhibited a macroporous structure with the pore diameter ranging from 100 to 300 μm. The average porosity of the 3D-GFs was determined to be 99.2%, while the width of the graphene strut walls was about 70–100 μm. The graphene strut walls were not solid but hollow in nature. The exact wall thickness is determined by the growth time, which in turn determines the density of the GF. Pettes[41] conducted TEM (transmission electron microscopy) imaging of the free

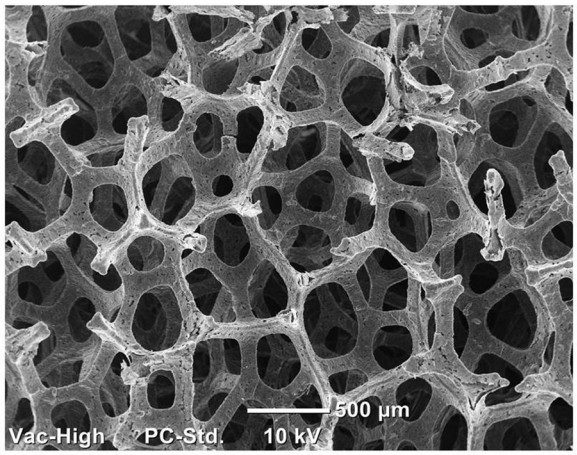

(a)

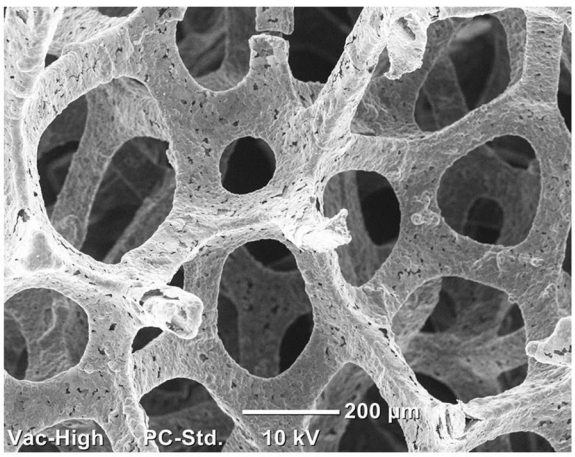

(b)

FIG. 4. SEM images of the GF before the NC deposition.

standing graphene samples and found the strut wall thickness to vary from 14 to 45 nm for densities ranging from 10 to 32 mg/cm^3.

Figure 5 shows the SEM images of the GF after the fuel deposition. The fuel loading is defined as the mass of the fuel per total mass of the system (fuel + GF). As shown in Fig. 5(a), corresponding to 75% fuel loading, not all pores were completely filled. This was expected since, based on the mass % of the fuel, only 5% of the total empty space of the GF matrix could be filled. This volume fill percentage number was, however, under-predicted as the hollow space inside the GF strut walls was not considered. With further decease in the fuel loading percentage, the morphology of the GF foam structure was more clearly visible, because of the decreased deposited fuel thickness on the strut walls (Figs. 5(a)–5(d)). Moreover, the number of GF pores that remained partially unfilled after the fuel deposition also increased with decreasing fuel concentration. Special precautions were made to make sure that during the deposition process, the fuel solution wets most the GF strut walls. This was done by decreasing the viscosity of the fuel solution so that it could easily enter the pores. Thus after the evaporation process, a thin layer of fuel was left coating the inner and outside areas of the GF walls, as can be seen in Figs. 5(e)

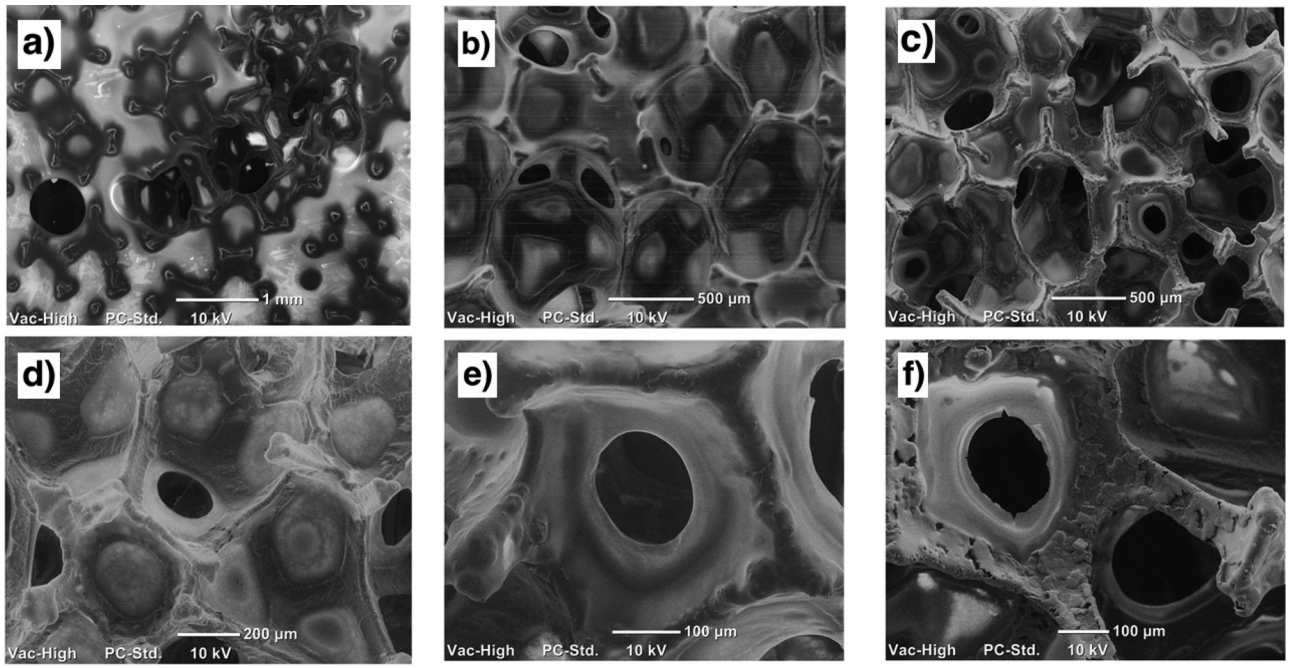

FIG. 5. SEM images of the GF (18 mg/cm^3) after the NC deposition. Low magnification images of (a) 75%, (b) 65%, (c) 55%, and (d) 45% fuel loading. High magnification images of (e) 55% and (f) 45% fuel loading.

and 5(f), thus providing an interconnected GF-NC network for the heat conduction during the combustion process.

B. Graphene nano-pellets (GNPs) results

As the GNPs were introduced into the fuel solution, the net thermal conductivity of the GNP-doped fuel samples was enhanced. The effective thermal conductivity of the GNPs-NC samples was measured experimentally using a steady state, controlled heat flux method based on the one dimensional heat flow between two parallel, isothermal reference materials separated by the GNPs-NC sample of uniform thickness. The reference material was polytetrafluoroethylene (PTFE) with a thermal conductivity of 0.3 W/mK. A thermal gradient was imposed across the GNPs-NC sample using a hot and a cold surface in contact with the reference materials. The temperature of the hot surface was maintained using an electric type heater with a constant voltage supply, while the temperature of the cold surface was maintained at a fixed temperature using the circulated cold water (20 °C). Three GNPs-NC samples having 0%, 2%, and 5% GNPs by weight were tested. The thickness of all the three samples was 1 mm. For each sample, three different measurements were made using three different heat fluxes (temperature ranges). The different heat fluxes were obtained by changing the temperature of the hot surface using the voltage supply, while keeping the temperature of the cold surface fixed at 20 °C. The temperature measurements were done using the IR (MWIR-1024) camera. Before the temperature measurements were performed, a calibration using the IR camera was done to get the emissivity values of the reference materials and the GNPs-NC samples. An effective thermal conductivity of 0.0952 ± 0.01 (W/mK), 0.1278 ± 0.01 (W/mK), and 0.164 ± 0.01 (W/mK) was obtained for GNPs-NC sample having 0%, 2%, and 5% GNPs by weight, respectively.

Fig. 6 shows that a linear increase in the K_{eff} values was obtained with a 70% enhancement for the GNPs-NC sample having 5% GNPs by weight. Thus, for low concentration of GNPs, the net effective thermal conductivity of the sample is not high enough to conduct heat efficiently from the exothermic reaction to aid reaction propagation. On the contrary, at high concentrations of GNPs, although the thermal conductivity of the GNP-doped NC complex was a lot higher, the amount of heat energy reaching the unburned portions of the fuel was substantially reduced because some of the energy released during the exothermic reaction was used in heating the GNPs, which acted as heat sinks and thus reduced the reaction propagation speeds. In addition, the surface morphologies of the deposited NC films (Fig. 3) can also affect the burn rate enhancements.[76,77] Consequently, an optimum concentration was obtained, as shown in Fig. 7. An optimum concentration of around 3% by weight was obtained for which the average

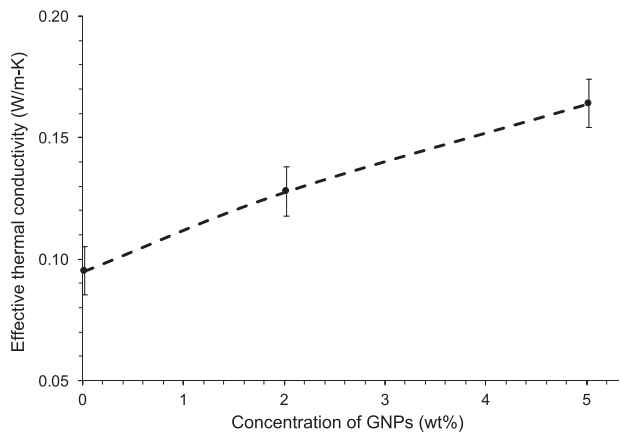

FIG. 6. Thermal conductivity measurements for GNPs-NC samples.

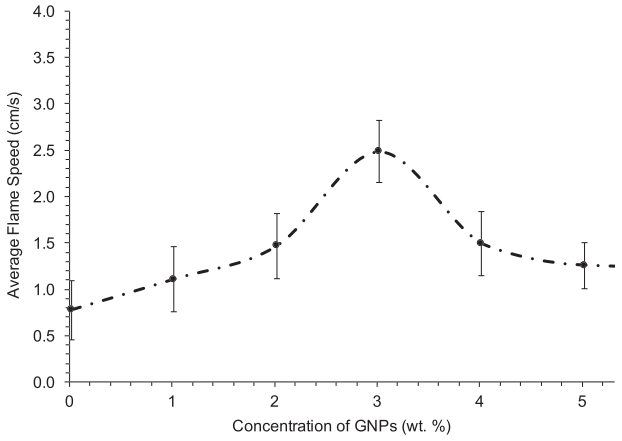

FIG. 7. The effect of the GNPs concentration on the average flame speed of NC (0% GNP corresponds to pure NC).

flame speed was around 2.3 cm/s (around 3 times the pure NC speed of 0.72 cm/s).

The SEM image of the top view of the fuel sample after combustion, Fig. 8(a), shows that the GNPs remained unburned after the combustion process but their 2-D structure was destroyed. This observation was consistent with the GNP's high temperature stability as shown by the thermogravimetric analysis (TGA in air) in Fig. 8(b), where only 10% of the weight loss was observed around 500 °C. The maximum temperature measured, using a k-type thermocouple, was around 600 K ± 10 K; thus, the thermal stability of the GNPs obtained was as expected.

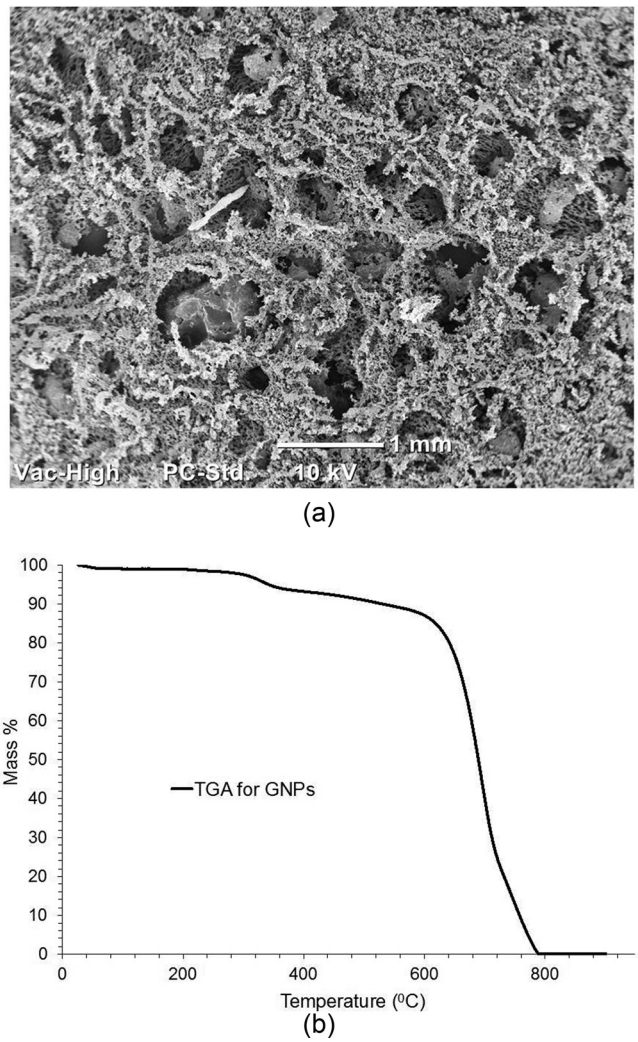

FIG. 8. (a) SEM image of the GNP-doped fuel sample after combustion. (b) TGA of the GNPs in air.

In our previous work,[74] coupled 1-D energy conservation equations along with simple one-step Arrhenius kinetics, similar to the 1-D model proposed by Mercer *et al.*,[78] were modelled to better understand the flame speed enhancements. The effect of the parameters such as the non-dimensional inverse adiabatic temperature rise and the effective thermal diffusivity on the flame speed propagation behavior was studied. The effective thermal diffusivity of the samples, the heat loss to the environment, and the heat produced were found to control the amount of flame speed enhancement obtained. For the present case of GNPs-NC complex, the effective density and specific heat capacity can be obtained as follows:[79]

$$(\rho c_p)_{eff} = \phi(\rho c_p)_G + (1-\phi)(\rho c_p)_f. \quad (1)$$

In the above equation, the subscript f refers to the fuel, whereas the subscript G refers to the GNPs. For the case of 5% by wt. GNPs added, only a 2% change in the $(\rho cp)_{eff}$ is obtained. This is in contrast to the effective thermal conductivity, where a 70% enhancement was obtained for 5% by weight GNPs. Thus, most of the enhancement observed in the effective thermal diffusivity (α_{eff}) of the GNPs-NC samples is from the effective thermal conductivity of the samples and the effects due to the changes in the densities and the specific heats are marginal. The enhancement in the α_{eff} leads to faster flame speed propagation, similar to the observations made in our previous work.[74]

To understand the relative importance of the convective heat transfer, a ratio between the conductive and the convective heat transfer[80] was calculated by performing an order of magnitude analysis of the variables involved. The conductive heat flux was found to be 10^3 times that of the convective heat flux; thus, the contribution of the convective heat transfer process could be ignored. This was similar to the observations made by Choi *et al.*[15] and Jain *et al.*[74]

C. Graphene foam (GF) results

Figure 9 shows the effect of the fuel loading % on the average flame speeds for a fixed foam density of 18 mg/cm^3. As can be seen, an optimum fuel loading of around 55% was obtained with flame speeds up to 4.5 cm/s (around 6 times the bulk NC speed of 0.72 cm/s). Compared to the GNPs, almost 2 times the enhancement was observed. This could be attributed to two factors. First of all, GF has been shown in previous studies to have the high basal-plane solid thermal conductivity of thin graphene while avoiding the thermal interface resistance issue found in GNPs and CNTs.[35,41,69,70] The TBR value can have a significant effect on the net effective thermal conductivity of the sample. Ji *et al.*[34] conducted a comprehensive study in which the thermal conductivity enhancement of wax using GF and GNPs was compared. GF was found to increase the thermal conductivity of the

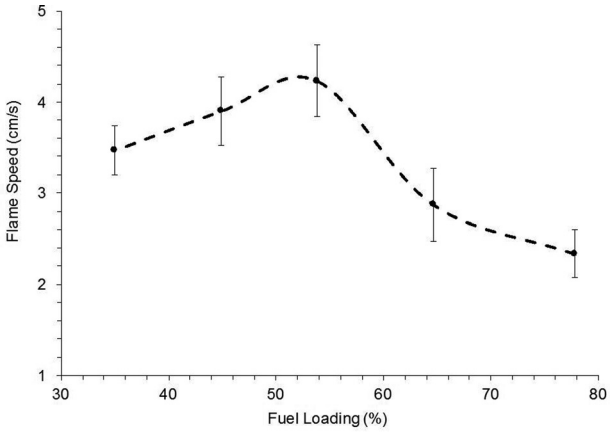

FIG. 9. The effect of the fuel loading on the average flame speed of NC. The foam density was fixed at 18 mg/cm^3.

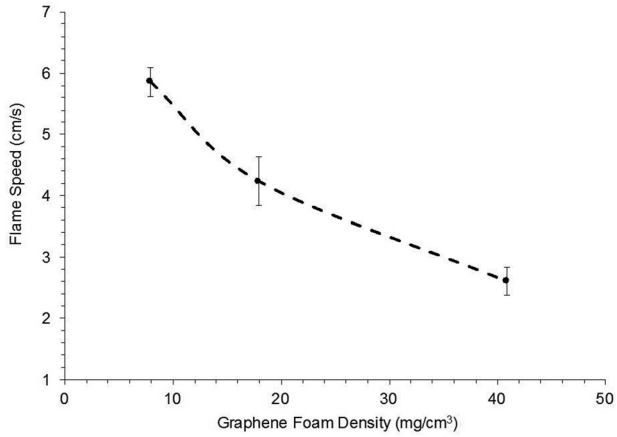

FIG. 10. The effect of the GF density on the average flame speeds. The fuel loading was fixed at 55%.

composite 18 times (1% vol.), which was much higher than the amount of enhancement observed using the GNPs (only 1.5 times for the same volumetric loading). Second, GF because of its inter-connected 3-D structure provides a continuous thermal conduction path, which does not exist in the case of GNP-doped fuel samples because of the random orientation of the GNPs. Since the GNPs are 2D carbon materials, the in-plane and through-plane thermal conductivities are significantly different.[81] For example, the GNP's in-plane and through-plane thermal conductivities have been measured to be around 3000 W/mK and 6 W/mK, respectively.[82] Thus, the thermal conduction in GNP-doped fuel sample is anisotropic and the orientation can have a significant effect on the net thermal conductivity enhancement. Moreover, in the flame propagation direction, the GNPs are not in direct contact with each other but have fuel in between, which tends to increase the TBR value even further. This is in contrast to GF, in which the graphene structure is connected from end to end with a thin fuel deposition around the GF strut walls (Fig. 5).

Figure 10 shows the effect of the GF density on the average flame speeds at the optimum fuel loading of 55%. For the GF of density 8 mg/cm^3, flame speeds up to 6 cm/s (around 8 times the bulk NC speed of 0.72 cm/s) were obtained, which was 300% greater than the flame speed obtained using the GF of density 40 mg/cm^3 and 260% greater than the maximum flame speed obtained using the GNPs. As can be seen, a monotonically decreasing trend was observed where the flame speed decreases with increasing GF density, which possibly could be due to the higher crystallographic defects observed in the higher density samples.

Figure 11 shows the SEM images of a low density and a high density samples. For the thick-walled higher density sample, the GF structure was more defective as can be seen from the increased surface roughness. This was consistent with the observations by Pettes *et al.*,[41] in which the surface morphologies of the GFs with different growth times (densities) were studied. The defect in the graphene structures can be characterized by looking at the ratio of the intensities of the disorder-induced D-band to the symmetry-allowed G-band ratio.[83] In graphene, the Stokes phonon energy shift caused by the laser excitation gives rise to three peaks in the Raman spectrum: G peak (1580 cm^{-1}), a primary in-plane vibrational mode, 2D peak (2690 cm^{-1}), a second-order overtone of a different in-plane vibration mode, and a D peak (1350 cm^{-1}), which is referred to as the defect-activated

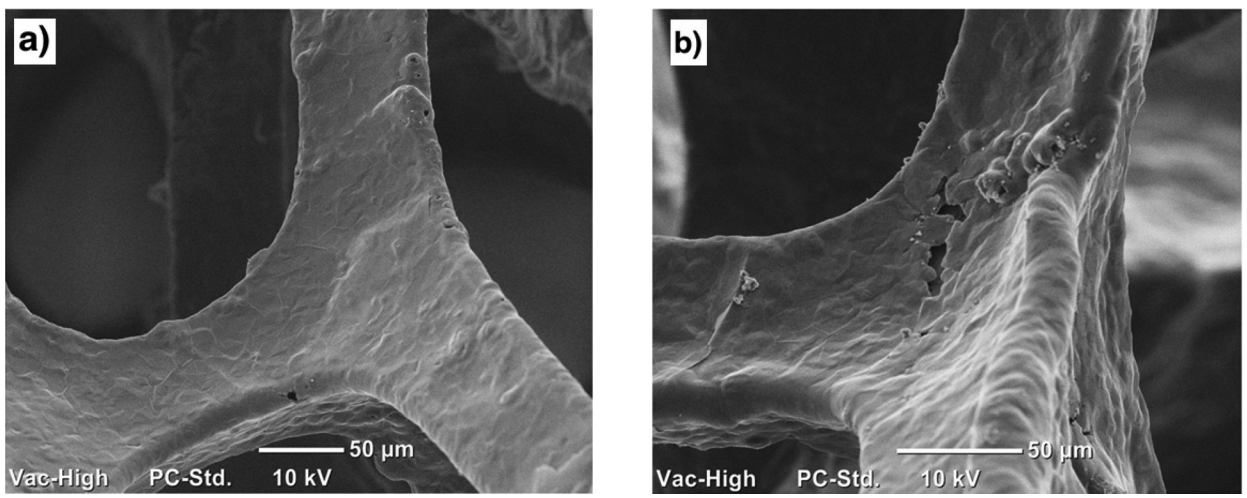

FIG. 11. SEM images of the strut walls of the GF with different densities, (a) 8 mg/cm^3 and (b) 18 mg/cm^3.

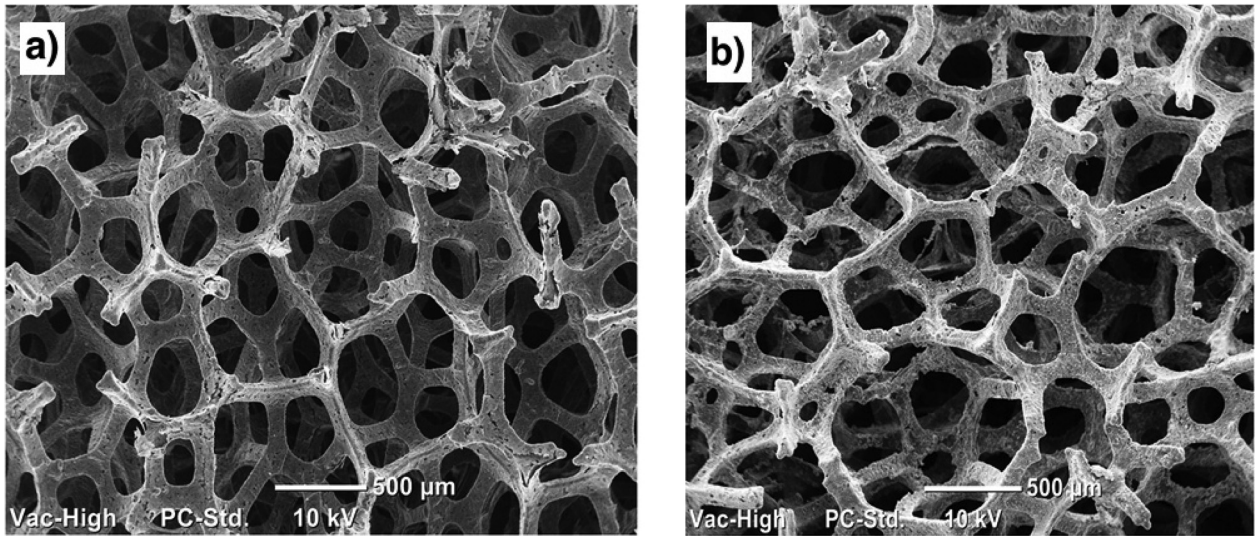

FIG. 12. SEM image of GF (a) before combustion; (b) after combustion. The particular case shown corresponds to GF of density 18 mg/cm^3 and fuel loading of 25%.

Raman mode.[79] Pettes *et al.*[41] perfomed the Raman spectroscopy of the strut walls of the GF samples and found that for the low density (11.6 mg/cm^3) samples, no observable D peak was observed, which matched well with those of the high quality graphene, signifying no defects. This was in contrast to the high density samples (31.7 mg/cm^3), where a D peak to G peak intensity ratio of 2% was observed. The surface defects can significantly affect the phonon scattering mean free path, which in turn can affect the thermal conductivity of the GF strut walls.[84] Pettes *et al.*[41] also measured the solid thermal conductivity of the GF walls and found the thermal conductivity value for the low density sample to be twice as much as that for the high density sample. Moreover, since the fuel was drop casted on to the GF surface, the surface roughness can have an additional effect of increasing the TBR value between the fuel and the GF strut walls, which could further decrease the effective thermal conductivity of the fuel-GF sample. Thus, all of the above effects combine to lower the flame speed for the high density samples more as compared to that of the low density samples.

Figure 12 shows the SEM image of the GF before and after combustion. Similar to the GNPs, the GF remained unburned after combustion, but in contrast to the GNPs, the 3D interconnected network of the GF was also preserved. Moreover, the TGA of pure GF was also conducted in air, and as shown in Fig. 13, only 5% of weight loss was observed at 600 °C. The maximum temperature of the GF observed during the combustion process was 600 K; thus, the thermal stability of the GF obtained was as expected. In addition, the reusability of the GF structure was also tested by re-depositing the GF surface with fuel. The particular case that was considered was with using the GF of density 18 mg/cm^3 and with the fuel loading of 25%. Similar flame speeds were obtained for the fresh and reused GF structure, respectively, implying that the thermal properties of the GF remained unchanged after the combustion process.

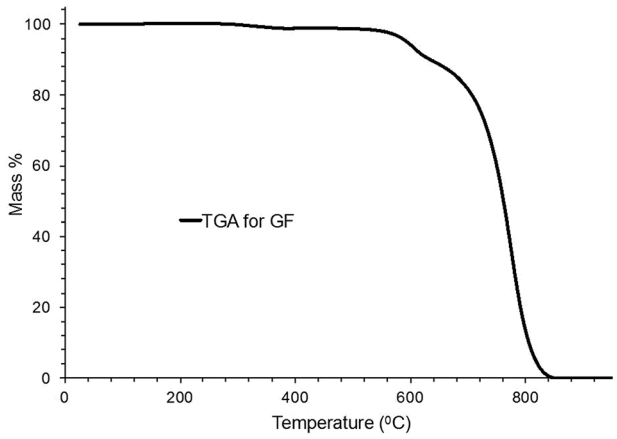

FIG. 13. TGA of GF (18 mg/cm^3) in air.

IV. CONCLUSIONS

In this study, the flame speed enhancement of a nitrocellulose solid monopropellant was shown to occur when coupled to highly conductive graphene structures including GNPs and GF. The high thermal conductivity of these structures facilitates the transfer of heat from the reaction zone to the unburned portions of the fuel, which sustains the propagating exothermic reaction front. For GNPs, the flame speeds were shown to be dependent upon the concentration of the GNPs added. An optimum GNP concentration at 3% was determined which gives the maximum enhancement, 3 times the bulk flame speed. For the GF structures, the effect of the fuel loading ratio % and the GF density on the average flame speeds were considered. An optimum fuel loading of around 55% was obtained with the flame speeds, showing a monotonic decreasing trend with increasing the GF density. Flame speed enhancements up to 8 times the bulk value were observed, which was 260% times greater than that obtained using the GNPs. Such a significant improvement was attributed to the GF's unique surface morphologies, which can lead to a difference in the thermal conductivities, contact resistances, and NC film surface roughnesses, all of which combine to alter the burn rate enhancements.[76,77] Finally,

both the GNPs and the GF remained unburned after the combustion process. The reusability of the GF structure was also tested by re-depositing it with fuel. Similar flame speed enhancements were obtained using the fresh and re-used GF structures.

[1]M. W. Beckstead, T. L. Boggs, and R. L. Derr, AIAA J. **8**, 370 (1970).
[2]A. Shalom, H. Aped, M. Kivity, and D. Horowitz, in 41st AIAA/ASME/SAE/ASEE Joint Propulsion Conference and Exhibit (American Institute of Aeronautics and Astronautics, 2005).
[3]K. Kishore and V. Gayathri, *Fundamentals of Solid-Propellant Combustion* (American Institute of Aeronautics and Astronautics, 1984), p. 53.
[4]G. Peter, Z. Chris, N. Roberto, and S. Steven, in 44th AIAA/ASME/SAE/ASEE Joint Propulsion Conference & Exhibit (American Institute of Aeronautics and Astronautics, 2008).
[5]Z. Ma, F. Li, and H. Bai, Propellants, Explos., Pyrotech. **31**, 447 (2006).
[6]I. P. S. Kapoor, P. Srivastava, and G. Singh, Propellants, Explos., Pyrotech. **34**, 351 (2009).
[7]Y. Wang, X. Xia, J. Zhu, Y. Li, X. Wang, and X. Hu, Combust. Sci. Technol. **183**, 154 (2010).
[8]P. R. Patil, V. N. Krishnamurthy, and S. S. Joshi, Propellants, Explos., Pyrotech. **31**, 442 (2006).
[9]W. Li and H. Cheng, J. Cent. South Univ. Technol. **14**, 291 (2007).
[10]A. Ünver, N. Dilsiz, M. Volkan, and G. Akovalı, J. Appl. Polym. Sci. **96**, 1654 (2005).
[11]G. M. Gore, R. G. Bhatewara, K. R. Tipare, A. N. Nazare, and S. N. Asthana, J. Propul. Power **20**, 758 (2004).
[12]W. Munson, R. Walker, and L. Mcgee, in 13th Propulsion Conference (American Institute of Aeronautics and Astronautics, 1977).
[13]F. Gilles and H. Bruno, in 30th Joint Propulsion Conference and Exhibit (American Institute of Aeronautics and Astronautics, 1994).
[14]T. D. Manship, M.S.A.A. thesis, Purdue University, 2010.
[15]W. Choi, S. Hong, J. T. Abrahamson, J.-H. Han, C. Song, N. Nair, S. Baik, and M. S. Strano, Nat. Mater. **9**, 423 (2010).
[16]P. Kim, L. Shi, A. Majumdar, and P. L. McEuen, Phys. Rev. Lett. **87**, 215502 (2001).
[17]L. M. Viculis, J. J. Mack, O. M. Mayer, H. T. Hahn, and R. B. Kaner, J. Mater. Chem. **15**, 974 (2005).
[18]Z. Chen, W. Ren, L. Gao, B. Liu, S. Pei, and H.-M. Cheng, Nat. Mater. **10**, 424 (2011).
[19]W. Cai, A. L. Moore, Y. Zhu, X. Li, S. Chen, L. Shi, and R. S. Ruoff, Nano Lett. **10**, 1645 (2010).
[20]S. Chen, A. L. Moore, W. Cai, J. W. Suk, J. An, C. Mishra, C. Amos, C. W. Magnuson, J. Kang, L. Shi, and R. S. Ruoff, ACS Nano **5**, 321 (2011).
[21]S. Ghosh, W. Bao, D. L. Nika, S. Subrina, E. P. Pokatilov, C. N. Lau, and A. A. Balandin, Nat. Mater. **9**, 555 (2010).
[22]S. Berber, Y.-K. Kwon, and D. Tománek, Phys. Rev. Lett. **84**, 4613 (2000).
[23]M. K. Samani, N. Khosravian, G. C. K. Chen, M. Shakerzadeh, D. Baillargeat, and B. K. Tay, Int. J. Therm. Sci. **62**, 40 (2012).
[24]K. Sun, M. A. Stroscio, and M. Dutta, J. Appl. Phys. **105**, 074316 (2009).
[25]I. Jung, D. A. Dikin, R. D. Piner, and R. S. Ruoff, Nano Lett. **8**, 4283 (2008).
[26]X. Li, G. Zhang, X. Bai, X. Sun, X. Wang, E. Wang, and H. Dai, Nat. Nanotechnol. **3**, 538 (2008).
[27]M. J. Biercuk, M. C. Llaguno, M. Radosavljevic, J. K. Hyun, A. T. Johnson, and J. E. Fischer, Appl. Phys. Lett. **80**, 2767 (2002).
[28]V. Goyal and A. A. Balandin, Appl. Phys. Lett. **100**, 073113 (2012).
[29]H. Huang, C. H. Liu, Y. Wu, and S. Fan, Adv. Mater. **17**, 1652 (2005).
[30]A. Yu, P. Ramesh, M. E. Itkis, E. Bekyarova, and R. C. Haddon, J. Phys. Chem. C **111**, 7565 (2007).
[31]F. Yavari, H. R. Fard, K. Pashayi, M. A. Rafiee, A. Zamiri, Z. Yu, R. Ozisik, T. Borca-Tasciuc, and N. Koratkar, J. Phys. Chem. C **115**, 8753 (2011).
[32]K. M. F. Shahil and A. A. Balandin, Nano Lett. **12**, 861 (2012).
[33]A. Yu, P. Ramesh, X. Sun, E. Bekyarova, M. E. Itkis, and R. C. Haddon, Adv. Mater. **20**, 4740 (2008).
[34]H. Ji, D. P. Sellan, M. T. Pettes, X. Kong, J. Ji, L. Shi, and R. S. Ruoff, Energy Environ. Sci. **7**, 1185 (2014).
[35]X. Zhang, K. K. Yeung, Z. Gao, J. Li, H. Sun, H. Xu, K. Zhang, M. Zhang, Z. Chen, M. M. F. Yuen, and S. Yang, Carbon **66**, 201 (2014).
[36]Z. Liu, D. Shen, J. Yu, W. Dai, C. Li, S. Du, N. Jiang, H. Li, and C.-T. Lin, RSC Adv. **6**, 22364 (2016).
[37]M.-T. Hung, O. Choi, Y. S. Ju, and H. T. Hahn, Appl. Phys. Lett. **89**, 023117 (2006).
[38]Y.-H. Zhao, Z.-K. Wu, and S.-L. Bai, Composites, Part A **72**, 200 (2015).
[39]M. B. Bryning, D. E. Milkie, M. F. Islam, J. M. Kikkawa, and A. G. Yodh, Appl. Phys. Lett. **87**, 161909 (2005).
[40]S. Harish, D. Orejon, Y. Takata, and M. Kohno, Appl. Therm. Eng. **80**, 205 (2015).
[41]M. T. Pettes, H. Ji, R. S. Ruoff, and L. Shi, Nano Lett. **12**, 2959 (2012).
[42]L. Chen, R. Zou, W. Xia, Z. Liu, Y. Shang, J. Zhu, Y. Wang, J. Lin, D. Xia, and A. Cao, ACS Nano **6**, 10884 (2012).
[43]J.-N. Shi, M.-D. Ger, Y.-M. Liu, Y.-C. Fan, N.-T. Wen, C.-K. Lin, and N.-W. Pu, Carbon **51**, 365 (2013).
[44]J. Xu and T. S. Fisher, Int. J. Heat Mass Transfer **49**, 1658 (2006).
[45]T. Tong, Y. Zhao, L. Delzeit, A. Kashani, M. Meyyappan, and A. Majumdar, IEEE Trans. Compon. Packag. Technol. **30**, 92 (2007).
[46]M. A. Panzer, G. Zhang, D. Mann, X. Hu, E. Pop, H. Dai, and K. E. Goodson, J. Heat Transfer **130**, 052401 (2008).
[47]W. Park, Y. Guo, X. Li, J. Hu, L. Liu, X. Ruan, and Y. P. Chen, J. Phys. Chem. C **119**, 26753 (2015).
[48]K. H. Baloch, N. Voskanian, M. Bronsgeest, and J. Cumings, Nat. Nanotechnol. **7**, 316 (2012).
[49]Z. Yan, G. Liu, J. M. Khan, and A. A. Balandin, Nat. Commun. **3**, 827 (2012).
[50]T. Cohen-Karni, Q. Qing, Q. Li, Y. Fang, and C. M. Lieber, Nano Lett. **10**, 1098 (2010).
[51]X. Dong, X. Wang, L. Wang, H. Song, H. Zhang, W. Huang, and P. Chen, ACS Appl. Mater. Interfaces **4**, 3129 (2012).
[52]X. Li, J. Warzywoda, and G. B. McKenna, Polymer **55**, 4976 (2014).
[53]Y. Liu, X. Dong, and P. Chen, Chem. Soc. Rev. **41**, 2283 (2012).
[54]G. Yang, C. Lee, J. Kim, F. Ren, and S. J. Pearton, Phys. Chem. Chem. Phys. **15**, 1798 (2013).
[55]H. Wang, Y. Yang, Y. Liang, J. T. Robinson, Y. Li, A. Jackson, Y. Cui, and H. Dai, Nano Lett. **11**, 2644 (2011).
[56]S. Nardecchia, D. Carriazo, M. L. Ferrer, M. C. Gutierrez, and F. del Monte, Chem. Soc. Rev. **42**, 794 (2013).
[57]Z.-S. Wu, Y. Sun, Y.-Z. Tan, S. Yang, X. Feng, and K. Müllen, J. Am. Chem. Soc. **134**, 19532 (2012).
[58]P. Bonnet, D. Sireude, B. Garnier, and O. Chauvet, Appl. Phys. Lett. **91**, 201910 (2007).
[59]A. Moisala, Q. Li, I. A. Kinloch, and A. H. Windle, Compos. Sci. Technol. **66**, 1285 (2006).
[60]S. T. Huxtable, D. G. Cahill, S. Shenogin, L. Xue, R. Ozisik, P. Barone, M. Usrey, M. S. Strano, G. Siddons, M. Shim, and P. Keblinski, Nat. Mater. **2**, 731 (2003).
[61]P. L. Kapitza, J. Phys. (Moscow) **4**, 181 (1941).
[62]N. Shenogina, S. Shenogin, L. Xue, and P. Keblinski, Appl. Phys. Lett. **87**, 133106 (2005).
[63]C.-W. Nan, G. Liu, Y. Lin, and M. Li, Appl. Phys. Lett. **85**, 3549 (2004).
[64]R. S. Prasher, X. J. Hu, Y. Chalopin, N. Mingo, K. Lofgreen, S. Volz, F. Cleri, and P. Keblinski, Phys. Rev. Lett. **102**, 105901 (2009).
[65]L. Hu, T. Desai, and P. Keblinski, J. Appl. Phys. **110**, 033517 (2011).
[66]K. Zhang, Y. Chai, M. M. F. Yuen, D. G. W. Xiao, and P. C. H. Chan, Nanotechnology **19**, 215706 (2008).
[67]Z. L. Gao, K. Zhang, and M. M. F. Yuen, Nanotechnology **22**, 265611 (2011).
[68]H. Chen, M. Chen, J. Di, G. Xu, H. Li, and Q. Li, J. Phys. Chem. C **116**, 3903 (2012).
[69]M. A. Raza, A. Westwood, and C. Stirling, Mater. Des. **85**, 67 (2015).
[70]X. Shen, Z. Wang, Y. Wu, X. Liu, Y.-B. He, and J.-K. Kim, Nano Lett. **16**, 3585 (2016).
[71]R. J. Heaston, European Research Office (United States Army), AD-815882, Frankfurt, Germany (1996).
[72]R. H. W. Waesche and J. Wenograd, Combust., Explos. Shock Waves **36**, 125 (2000).
[73]J. F. Baytos, Los Alamos National Laboratory Informal Report No. LA-8034-MS, Los Alamos, New Mexico, 1979.
[74]S. Jain, O. Yehia, and L. Qiao, J. Appl. Phys. **119**, 094904 (2016).
[75]X. Zhang, W. M. Hikal, Y. Zhang, S. K. Bhattacharia, L. Li, S. Panditrao, S. Wang, and B. L. Weeks, Appl. Phys. Lett. **102**, 141905 (2013).
[76]X. Zhang, K. S. Ziemer, K. Zhang, D. Ramirez, L. Li, S. Wang, L. J. Hope-Weeks, and B. L. Weeks, ACS Appl. Mater. Interfaces **7**, 1057 (2015).

[77]X. Zhang and B. L. Weeks, J. Hazard. Mater. **268**, 224 (2014).
[78]G. N. Mercer, R. O. Weber, and H. S. Sidhu, Proc. R. Soc. London, Ser. A **454**, 2015 (1998).
[79]W. Guo, C. J. Lim, X. Bi, S. Sokhansanj, and S. Melin, Fuel **103**, 347 (2013).
[80]M. R. Weismiller, J. Y. Malchi, R. A. Yetter, and T. J. Foley, Proc. Combust. Inst. **32**, 1895 (2009).
[81]H. S. Kim, H. S. Bae, J. Yu, and S. Y. Kim, Sci. Rep. **6**, 26825 (2016).
[82]S. Y. Kim, Y. J. Noh, and J. Yu, Composites, Part A **69**, 219 (2015).
[83]J. I. Jang, *New Developments in Photon and Materials Research* (Nova Science Publishers, New York, 2013), pp. 403–418.
[84]G. Chen, *Nanoscale Energy Transport and Conversion: A Parallel Treatment of Electrons, Molecules, Phonons, and Photons* (Oxford University Press, New York, 2005).